npj | regenerative medicine

Article

Published in partnership with the Australian Regenerative Medicine Institute

https://doi.org/10.1038/s41536-025-00427-w

Human iPSCs-derived mesenchymal stem cells promote skin regeneration and burn wound healing

Mahmoud Farahat[1,2,8], Sophie Brosset[3,4,8], Yufei Chen[1,2], Ayesha Aijaz[1,2], Graham Rix[2], Bhavishya Challagundla[2], Margarita Elloso[1,2,5], Maria Fernanda Hutter[1,2,6], Ian M. Rogers[7] & Marc G. Jeschke[1,2,5] ✉

The key to surviving severe burns is rapid burn wound excision and closure, yet extensive wounds often surpass natural healing capacity. Alternative treatments, such as synthetic skin substitutes, have not emerged as a standard, optimal solution. Stem cell therapies, especially using allogenic sources, show promise in enhancing wound repair. Induced mesenchymal stem cells (iMSCs) have demonstrated vast possibilities to overcome traditional stem cell therapy limitations. This study utilized Cord tissue-derived iMSCs (CT-iMSCs) incorporated into well-established epidermal-dermal substitutes Integra® Dermal Regeneration Template (DRT) at 5000–20,000 cells/cm^2 in a porcine full-thickness burn model to test their regenerative capabilities. We evaluated healing outcomes, inflammation, neovascularization, collagen levels, and fibrosis markers. Wounds treated with CT-iMSCs showed notable improvements, including faster wound healing, better epithelialization, and marked improvements in healing markers compared to controls. These data support the potential of iMSCs as an ideal cell source for autologous skin regeneration.

Major burns are one of the most critical forms of injuries, annually contributing to more than 200,000 fatalities worldwide, either due to the burns themselves or burn-associated complications[1]. Most frequently, the substantial tissue loss and potential infection route caused by the burn injury leads to sepsis, constituting a major detrimental burn complication putting patients at higher risk of morbidities and death. Therefore, standardized critical burn care protocols prioritize the rapid surgical removal of burned skin and immediate wound coverage utilizing autologous skin grafting to ensure the survival of burn patients[2]. Though considered the gold standard, this therapeutic intervention has significant limitations, including creating a new wound site secondary to donor skin harvesting, limited availability of donor sites in extensive burns, and the risk of graft failure due to bacterial load on the wound bed[3]. Over the years, alternative skin substitutes have been introduced and applied to serve as wound coverage, including the widely used Integra®, a synthetic bilayer composed of a bottom matrix of bovine collagen I cross-linked with shark cartilage and an upper silicone protective layer. These skin substitutes function as a dermal regeneration template (DRT) to encourage intrinsic wound healing processes through endogenous cellular growth and subsequent tissue synthesis primarily organized by native stem cells[4].

The immense progress in stem cell therapy has represented a paradigm shift in medical practice for organ and tissue damage treatment. Mesenchymal stem cells (MSCs), the umbrella term that encompasses a population of multipotent stem cells (e.g., bone marrow, adipose, and umbilical cord), have demonstrated significant efficacy in the improvement of healing outcomes in terms of acceleration of the healing process, inducing scarless healing, reducing inflammation, and stimulating angiogenesis for acute/chronic wound treatment. Various primary stem cells have been tested in these trials without a particular source standing out as an ideal candidate. Limitations regarding the feasibility of autologous stem cell isolation, culture, and expansion, as well as immune rejection of allogeneic stem cells[5], remain posing serious impediments that hinder the effective translational use of stem cell therapy in burn patients, despite some breakthroughs that were achieved by our group and others[6,7].

[1]Department of Surgery, McMaster University, Hamilton, ON, Canada. [2]Centre for Burn Research, Hamilton Health Sciences, Hamilton, ON, Canada. [3]Sunnybrook Research Institute, Toronto, ON, Canada. [4]Department of Plastic and Reconstructive Surgery, Croix Rousse Hospital, Hospices Civils de Lyon, University Claude Bernard Lyon 1, Villeurbanne, Lyon, France. [5]Hamilton General Hospital, Hamilton Health Sciences, Hamilton, ON, Canada. [6]Division of Plastic, Aesthetic and Reconstructive Surgery, Department of Surgery, Medical University of Graz, Graz, Austria. [7]Division of Reproductive Sciences, Fran and Lawrence Bloomberg Department of Obstetrics and Gynecology, Lunenfeld Tanenbaum Research Institute, Mount Sinai Hospital and The University of Toronto, Toronto, ON, Canada. [8]These authors contributed equally: Mahmoud Farahat, Sophie Brosset. ✉e-mail: marc.jeschke@hhsc.ca

In this context, we have discovered that the often-excised and discarded burned skin harbors a population of viable stem cells termed burn-derived stem cells or BD-MSCs, which could be effectively isolated, characterized, and tested in the treatment of burns in a porcine full-thickness induced-burn model[8]. Data from an in vivo burn model showed that BD-MSCs significantly accelerated the wound healing time, reduced scar formation, and enhanced neovascularization at the wound site when applied on Integra® sheets to cover the burn wounds[9]. While utilization of BD-MSCs may effectively overcome the immune rejection impediment, the limited cell number obtained from tissues and restrained in vitro proliferation capacity against the enormous numbers of cells required for treating more extensive wounds, in addition to the impairment of therapeutic effectiveness of MSCs with age still pose major hurdles[10,11]. The development of induced pluripotent stem cell (iPSC) technology has revolutionized stem cell therapy and generated widespread enthusiasm about its utilization in regenerative medicine[12,13]. In principle, human iPSCs can differentiate into all somatic cells, including MSCs[14]. These iPSC-derived MSCs (iMSCs) show MSC-like phenotypes, including the expression of MSC-specific markers, being plastic adherent, and multipotent multilineage differentiation into osteo-, chondro-, and adipogenic lineages, which collectively fulfill the minimal MSCs criteria as defined by the International Society for Cellular Therapy (ISCT standard)[15]. Such differentiation capability provides a golden opportunity to prevail over the aforementioned translational limitations of primary MSCs since iPSCs can act as a potentially unlimited source for MSC differentiation, and most importantly, iMSCs can evade triggering adverse immunogenic reactions[16,17]. Compared to the most widely used primary MSCs, bone marrow-, adipose-, and umbilical cord tissue-derived MSCs (BM-MSCs, AD-MSCs, and CT-MSCs, respectively), iMSCs displayed superior therapeutic and immunomodulatory potential, especially compared to BM-MSCs and AD-MSCs, while showing similar marker expression and differentiation capacity.[18–20]

This led us to investigate the therapeutic effectiveness of iMSCs derived from cord tissue-iPSCs (CT-iPSCs) in promoting wound healing and skin regeneration in our established porcine thermal injury model. An MSC differentiation protocol was conducted to generate CT-iMSCs from a pre-established, validated CT-iPSC line. CT-iMSCs were applied to a well-recognized porcine thermal injury model, where they displayed superior healing outcomes compared to the control groups. These data could transform the burn care practice and provide hope for millions of burn patients.

Results

Establishment and characterization of iMSC

Figure 1 represents the schematic of the study flow, outlining the main steps and methods used throughout the research. Mohamed et al. previously demonstrated that human cord-tissue stem cells can be reprogrammed into induced pluripotent stem cells (CT-MSC-iPSCs). These cells were fully characterized through standard assays showing the expression of pluripotency markers Nanog, Oct4, and Sox2. In addition, they showed the ability to differentiate into the three germ layers (ectoderm, mesoderm, and endoderm) in vitro, and finally, they successfully formed tumors when injected subcutaneously in nude mice[21]. CT-MSC-iPSCs, here termed CT-iPSCs, were generously donated to us by Dr. Ian Rogers, University of Toronto, Canada. To confirm that cells retained their pluripotency, immunofluorescence and flow cytometry analyses were conducted, showing that the cells positively expressed pluripotency markers Nanog, Sox2, and TRA-1–60, respectively (Supplementary Fig. 1A, B). Next, a previously published protocol was utilized to induce the differentiation of CT-iPSCs into iPSCs-induced MSCs or iMSCs[22]. Cells were kept in a mesodermal induction medium for three days, before switching to MSCs induction medium for another ten days. As shown in supplementary Fig. 1, the expression of mesodermal markers Eomesodermin (Eomes) and MIXL1 was markedly enhanced by day 7, suggesting early differentiation of CT-iPSCs towards mesodermal derivatives (Supplementary Fig. 1C, D)[23,24]. Cells further differentiated into CD105 +, CD73 +, CD90 +, CD45− MSCs (Fig. 2A). Differentiated cells showed apparent morphological changes adopting the characteristic plastic adherent spindle shape (Fig. 2B). Additionally, the multi-differentiation capacity into adipocytes, osteoblasts, and chondrocytes was confirmed through staining analysis with Oil-Red-O, Alcian Blue, and Alizarin Red staining (Fig. 2C). Collectively, these results suggested that the CT-iPSCs were efficiently induced to mesodermal-lineage cells that could be furtherly differentiated into functional MSCs in vitro.

iMSCs accelerated burn wound healing in the porcine thermal injury model

After positively characterizing the nature of iMSC, A well-established porcine thermal injury model was used to assess their in vivo therapeutic effectiveness[9]. Previously, it was shown that MSCs could be effectively incorporated into Integra®, an FDA-approved, synthetic meshed bilayer wound coverage material scaffold for burn wound treatment[9,25]. Therefore, a similar protocol to incorporate iMSCs into Integra® was applied. The successful seeding of iMSCs onto Integra® was visually assessed by the absence of floating cells, confirming full incorporation and attachment to the scaffold before application to the experimental animal. Next, scaffolds containing iMSCs were placed on the 5 × 5 cm full-thickness excisional wounds as previously described. Notably, no adverse events related to the treatments, such as local or systemic signs of inflammation or infection, were observed throughout the experiment.

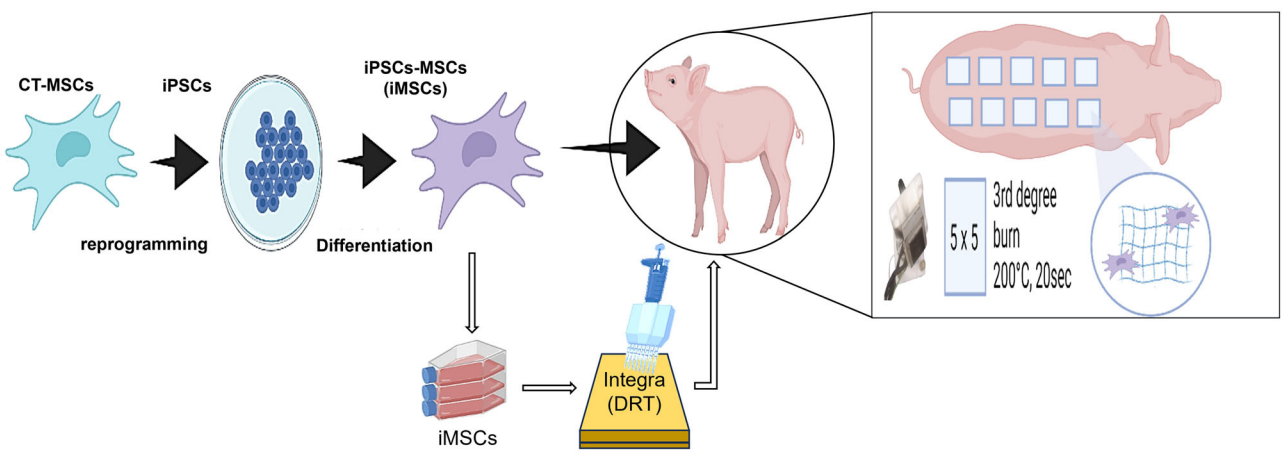

Fig. 1 | Schematic illustration depicting the study workflow. Isolated human CT-MSCs were reprogrammed to CT-iPSCs and further differentiated to iMSCs. These were expanded and seeded onto Integra DRT for application and testing in our porcine thermal injury model. *Created with BioRender.com.*

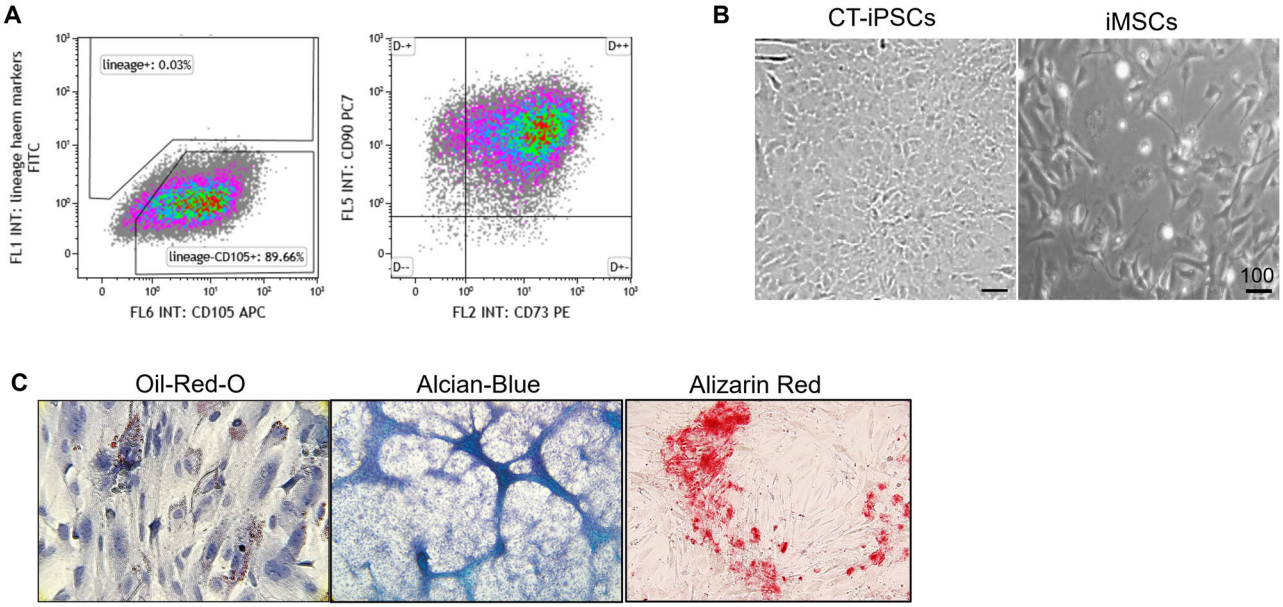

Fig. 2 | Characterization of the induced Mesenchymal stem cells (iMSCs). A Flow cytometry plot showing cell-positive expression of multipotency markers. CD105 + /CD4- cells were gated and sorted. Then, CD105+ cells were gated for CD73+ and CD90 + . **B** Bright field image showing the morphological changes of CT-iPSCs from round, in colony appearance, to spindle-shaped iMSCs. **C** Differentiated iMSCs exhibit multilineage differentiation capacity: Chondroblast (Alcian-Blue), Adipocyte (oil-Red-O), and Osteoblasts (Alizarin Red).

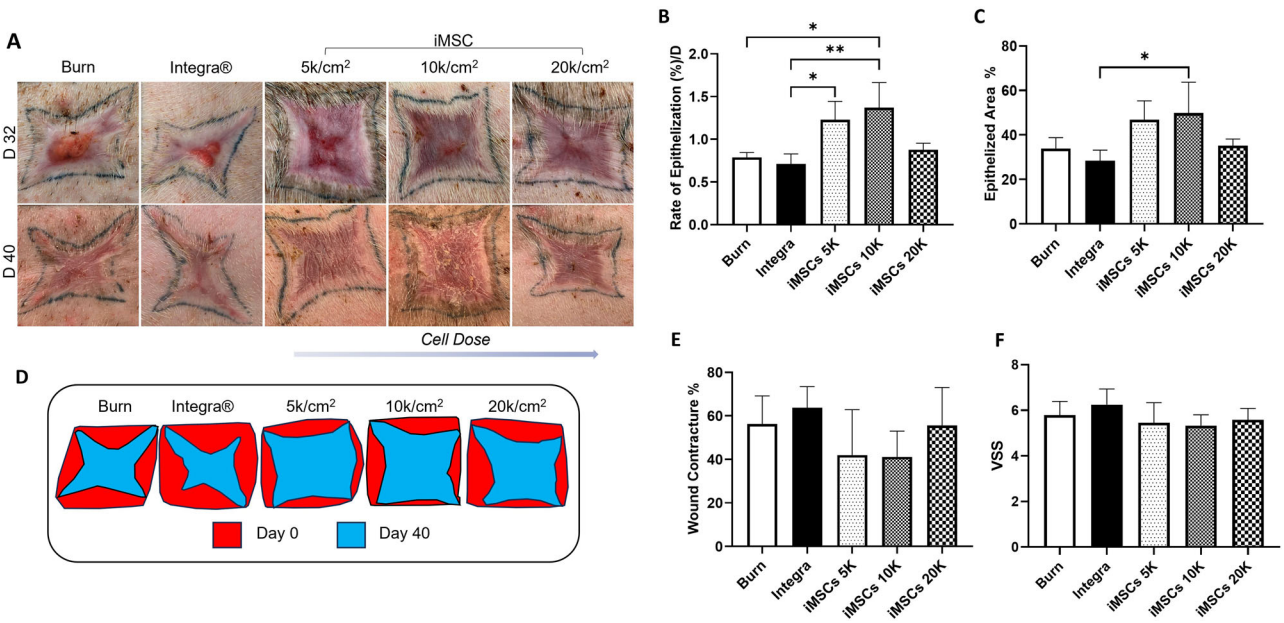

Fig. 3 | iMSCs improve the quality of wound healing. A Macroscopic images of wounds on days 32 and 40 post-burn. On day 32, iMSCs-treated wounds exhibited complete wound closure, by day 32 while both control and acellular Integra groups still showed open wounds. By Day 40, all wounds showed complete closure. Black lines represent the initial dimensions of the excised wounds. **B**, **C** Statistical analysis of rate and the total amount of neo-epithelization, 10 K/cm^2 iMSCS showed the highest levels compared to control groups. **D** simulated wound map displaying wound edge contraction. **E** Wound contracture rate analysis. iMSCs 5 and 10 K/cm^2 show the lowest contraction. **F** Vancouver scar scale scoring, control wounds showed a slight, nonsignificant increase compared to the iMSCS-treated wound. Data is representative of three independent experiments ($N = 3$). Data presented as mean ± SEM, P * < 0.05, ** < 0.005, $N = 3$.

Interestingly, gross wound analysis showed that all iMSC-treated wounds exhibited an accelerated wound closure as early as 32 days post-burn compared to burn alone and acellular Integra groups (Fig. 3A, and Supplementary Fig. 2A, B). However, all wounds showed a complete closure by day 40 (sacrifice day). Interestingly, analysis of the wound closure rate over the 40 days treatment period showed that the control groups showed an initial accelerated closure rate up to 12 days post burn, however, iMSCs-treated groups displayed a notable accelerated closure rate during the re-epithelization period (approximately between days 12–25 post-burn) suggesting a direct effect of the seeded stem cells on the epithelization process (Supplementary Fig. 2A, B). Indeed, analysis of the rate of

epithelization significantly increased in 5K-iMSC and 10K-iMSC groups compared to burn and acellular Integra groups (Fig. 3B). Further, the 10K-iMSCs exhibited the largest re-epithelialized area, significantly higher compared to the acellular Integra (Fig. 3C). Of note, the extent of re-epithelialization was assessed after removal of the silicone (bi-) layer of Integra® between days 10 and 14. Scarring susceptibility is another key factor in wound healing assessment. Scar quality on day 40 was assessed by evaluating the rate of wound contracture and the Vancouver Scar Scale (VSS) score. The analysis of macroscopic images suggested a manifested decrease in wound contraction in iMSCs-treated wounds relative to the control wounds (burn and acellular Integra) (Fig. 3 A and D). Furthermore, quantitative analysis revealed that both the 5K-iMSC and 10K-iMSC groups exhibited the lowest contracture rates, although the differences were not statistically significant (Fig. 3E). Nevertheless, no statistically significant differences in VSS scores were observed between groups; scar scores were higher in burn (6.67 ± 1.0) and acellular Integra (6.00 ± 0.57) compared to 5K-iMSCs (5.58 ± 0.91), 10K-iMSCs (5.33 ± 1.47), and 20K- iMSCs (6.00 ± 0.54) (Fig. 3F).

On the other hand, granulation tissue formation is an important step in the wound healing process. Wounds were scored for the presence, feature, and amount of granulation tissue throughout healing using the Bates-Jensen Wound Assessment tool[26]. Scores range were as follows 1 = Skin intact or partial thickness wound, 2 = Bright, beefy red; 75% to 100% of wound filled and/or tissue overgrowth, 3 = Bright, beefy red; < 75% and > 25% of wound filled 4 = Pink, and/or dull, dusky red and/or fills < 25% of wound, 5 = No granulation tissue present. By postburn day 4, no apparent granulation tissue deposition was observed in all groups. However, the collagen layer of the Integra templates was seen to integrate into wounds with no significant differences in iMCS-seeded groups compared to controls (burn and acellular Integra). Between postburn days 9–12, all wounds showed the presence of granulation tissue covering between 75 and 100% of the total wound area (Supplementary Fig. 2C). Upon entering into the reepithelialization phase, granulation tissue in iMCS-seeded groups started to be replaced by intact new epithelial tissue as reflected in granulation tissue scores (Supplementary Fig. 2C). In particular, 10 k/cm^2 iMSCs showed a steady increase in the score, indicating an improved wound-healing process that matched the wound closure course (Supplementary Fig. 2C).

iMSCs effectively restore wound tissue morphological features

Next, we sought to evaluate the wound tissue morphology. Wound tissue sections were stained for hematoxylin and eosin. A distinct skin morphology consisting of epidermis and dermis layers could be observed in wounds of all groups (Fig. 4A). Interestingly, apart from 10 k/cm^2 iMSCs, all groups showed a significant increase in epidermis thickness relative to the non-burned porcine skin (normal skin) (Fig. 4C). All groups demonstrated visibly apparent layers of epidermis; stratum corneum, stratum lucidum, stratum granulosum, and stratum basale being distinctive (Fig. 4A- lower magnified panel). The stratum corneum was noticeable as the uppermost flattened keratinocyte layer containing a dense network of keratin that varied in thickness between different groups. Acellular Integra and iMSCs 20 K/cm^2 showed a thicker keratin layer than the 5 and 10 K iMSCs groups. An underlying transparent stratum lucidum layer could be observed especially in the Integra group followed by the Stratum Basale as the dense deepest layer of the epidermis (Fig. 4A-middle panel). Close examination showed that wounds treated with 10 k/cm^2 iMSCs demonstrated a histological morphology of the epidermis most comparable to non-burned skin (Fig. 4A-lower magnified panel). Subsequently, the formation of rete ridges, the epithelial protrusion at the junction between epidermis and dermis, was quantified in wound histological sections. Control groups (burn and acellular Integra) followed by 20K-iMSCs had the lowest number of rete ridges, a statistically significant difference compared to 5K-iMSCs, 10K-iMSCs, and non-burned skin. The average number of ridges was 3.8 ± 1 and 4.3 ± 0.83 for burn and acellular Integra groups, respectively (Fig. 4D). While the average number of ridges in iMSCs wounds at 5 k/cm^2 = 7.6 ± 1, 10 k/cm^2 = 10.2 ± 0.83, and 20 k/cm^2 = 4 ± 1 per 1 mm (Fig. 4D). Notably, wounds treated with 10K-iMSCs exhibited rete ridges formation most comparable to non-burned skin (10.2 ± 0.83 and 12.8 ± 1.2, respectively). Dermis layer regeneration was then analyzed. Histologically, the dermis is a mainly fibrous connective tissue layer with a predominant collagen component and an embedded cellular population of fibroblasts, macrophages, and mast cells. Therefore, we analyzed wound samples with Mason-trichrome staining. Interestingly, acellular Integra wounds exhibited apparent hyperplasia in the dermis (Supplementary Fig. 3A, B) with an average of $53 \times 10^3 \pm 6700$ cells per mm^2. On the other hand, 20k followed by 10 K iMSCs groups showed the most comparable cell number compared to the non-burned skin ($44 \times 10^3 \pm 2500$, $40.8 \times 10^3 \pm 6613$, and $45.5 \times 10^3 \pm 7770$ cells per mm^2, respectively (Supplementary Fig. 3B). Additionally, 10k iMSCs-treated wounds had the highest collagen deposition, followed by 5 K iMSCs wounds (66 ± 15 and 56 ± 12% of total area), significantly higher than the burn and acellular Integra (22 ± 12 and 33 ± 8%), respectively; however, lower than the non-burned skin 78 ± 5.3 (Fig. 4E). Collectively, these histological assessments demonstrated that iMSCs treatment could improve the healing skin tendency for restoration of the natural skin features including both dermis and epidermis layers. In particular, a 10 K iMSCs dose tends to produce better wound healing outcomes and restore the skin histological features (Supplementary Fig. 3C).

iMSCs regulate inflammation and remodeling marker expression

To investigate iMSC-mediated mechanisms in wound repair, we analyzed the expression of key wound-healing–associated markers starting with major pro-inflammatory cytokines; IL1β, IL4, IL6, TNF-α, and growth factor; TGFβ3[27]. Interestingly, all iMSC-treated wounds exhibited reduced IL-1β expression compared to the burn control, with the 10 K iMSC group showing a statistically significant decrease (Fig. 5A). Similar patterns were observed for IL-4 and TNF-α, with the 10 K iMSC group again displaying the lowest, though not statistically significant, expression levels (Fig. 5B and Supplementary Fig. 4A). Likewise, for IL-6 and TGF-β3, the 10 K iMSC group showed the lowest expression among all treated groups, albeit without statistical significance, whereas the other iMSC-treated and acellular Integra groups exhibited expression levels comparable to the burn control (Fig. 5C, D). Further, we analyzed the expression of the two major dermal collagens: Collagen 1 and 3. Notably, all iMSCs-treated wounds exhibited a comparable non-significant 2.5-fold increase in the expression of Collagen 1α1 compared to the burn control Fig. 5E). However, Collagen 3A1 expression was similar across groups, with 5 K and 10 K iMSCs groups exhibiting slightly higher and lower expression, respectively (Fig. 5F). Replacement of collagen 3 with collagen 1 is particularly important for sound wound healing. Therefore, our evaluation showed that the 10 K iMSCs group had the highest Collagen1/3 ratio followed by acellular Integra and 5 K iMSCs groups (Supplementary Fig. 4B). Since collagen deposition is regulated by the action of the matrix metalloproteinases (MMPs) and their tissue inhibitors of metalloproteinases (TIMPS), we evaluated how major MMPs might be regulated with iMSCs treatment. Interestingly, wounds treated with iMSCs (5 and 20 K) showed a significantly higher MMP2 expression than burn and acellular Integra controls (Fig. 5G). On the contrary, they showed a significant decrease in MMP9 expression (Fig. 5H). Interestingly, plasminogen activator inhibitor-1 (PAI-1; SERPINE1), expression was increased in 5K-iMSC and 10K-iMSCs-treated wounds; significantly increased in 5 and 10 K while nonsignificant in the 20 K group (Supplementary Fig. 4C). Finally, to analyze the angiogenic potential of iMSCs, we analyzed the expression of the extracellular matrix (ECM)

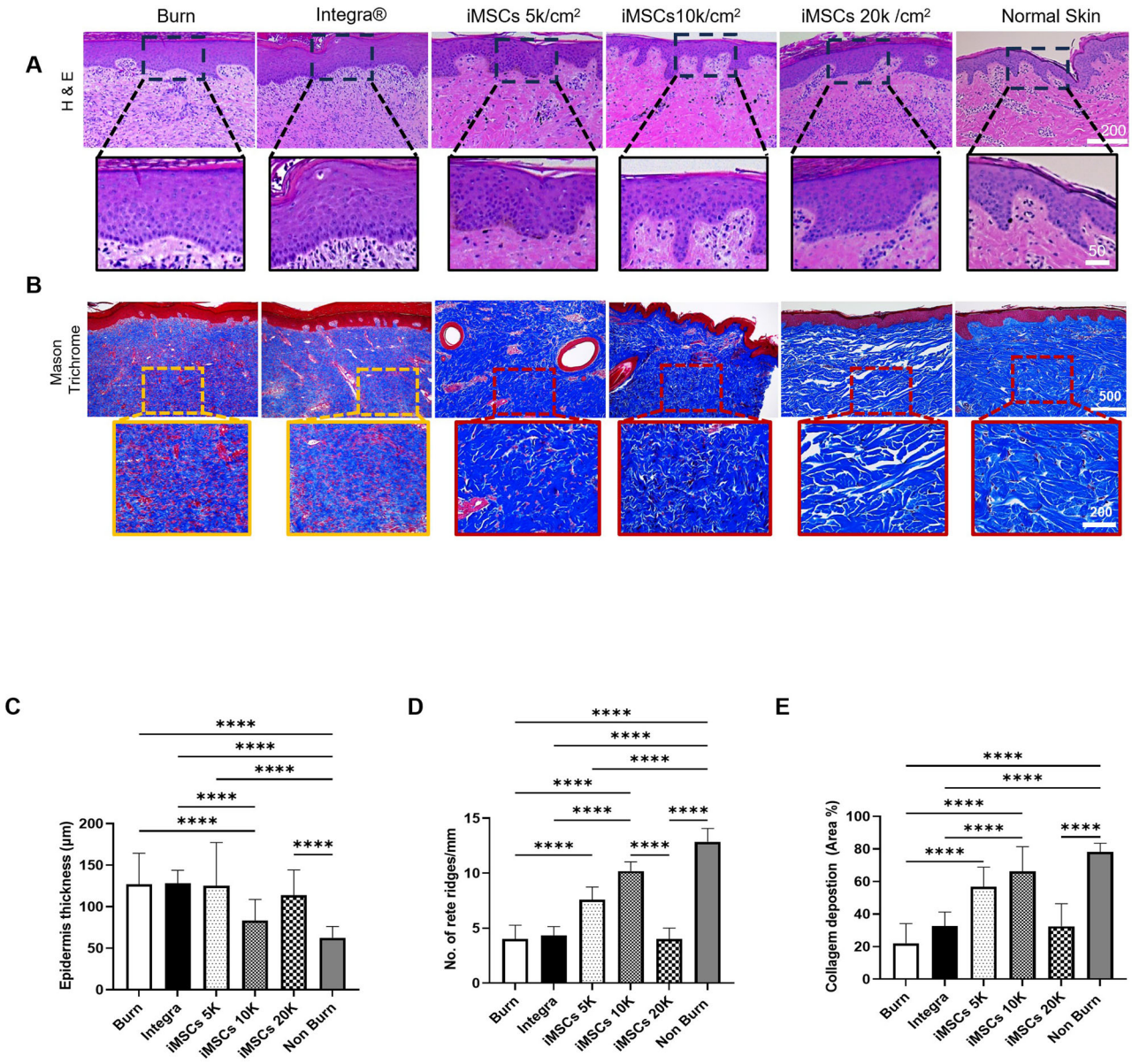

Fig. 4 | iMSCs treatment restores skin histological features. A Histological sections from healing wounds stained for H&E (Upper panel scale bar= 200 µm) (Lower panel scale bar= 50 µm). and (**B**) Mason's trichrome (Upper panel scale bar= 500 µm) (Lower panel scale bar= 200 µm). **C** Statistical analysis of average epidermis thickness. **D** Statistical analysis of the average number rete ridges per 1 mm **E** Statistical analysis of average collagen deposition. Data is representative of three independent experiments ($N = 3$). Data presented as ± SEM, P *** <0.0005, **** <0.0001.

glycoprotein Tenascin-C (TNC) and vascular endothelial growth factor (VEGF), essential for angiogenesis during wound healing. All iMSCs groups showed a 2-fold increase of TNC compared to the burn group (Supplementary Fig. 4D) and a slight increase of VEGF in 5 and 10 K iMSCs groups, though all changes were statistically non-significant (Supplementary Fig. 4E).

Together, these data showed that treatment with iMSCs enhanced burn wound healing outcomes that could be attributed to a general improvement in the expression of major molecules associated with different stages of wound healing. Particularly, a dose of 10 K iMSCs/cm^2 tends to produce lower inflammatory, higher collagen, and more angiogenic markers gene expressions which could be translated into better overall healing features.

Discussion

Recently, stem cell therapy has been perceived as the epitome of regenerative medicine and an integral part of modern medical care. However, one field has been lagging in the translational employment of stem cells, that is, burn wound treatment. Although some breakthroughs have been introduced into practice, a universal agreement on the effective stem cell source, dosage, application method, and mode of action is still far from being achieved. In a series of reports, we previously showed the therapeutic potential of different stem cell sources in burn wound healing[9,25,28]. In the present work, we demonstrated that MSCs differentiated from reprogrammed CT-iPSCs can be utilized as a promising stem cell source for treating burn injuries.

The criticality of burn injuries correlates with but is not limited to their destructive nature; rather, complex factors interact to determine survivability and prognosis. On top of these factors, rapid wound coverage proves to be one of the most determining aspects. Failure to adequately excise the burned skin and to cover the resulting wound, infection, and sepsis will ensue as common morbidities leading to substantially increased mortality[29]. Therefore, not only does burn treatment represent a race against injury, infection, and inflammation, but also against time. What makes burns specifically an aggravated form of injury is that, while in the case of other

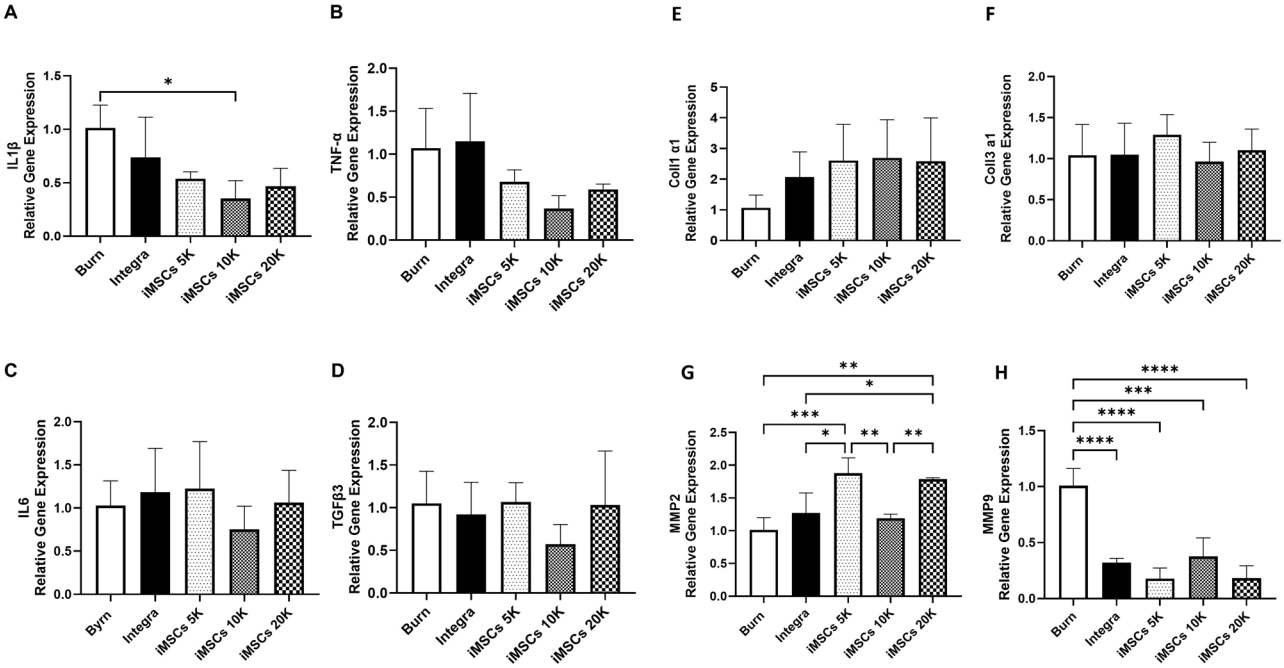

Fig. 5 | iMSCs modulation of wound healing markers. A–D iMSCs treatment suppresses major proinflammatory mediators (**A**) IL1β, (**B**) TNF-α, (**C**) IL6, and (**D**) TGFβ3. **E**, **F** iMSCs-treated wounds showed a marked increase in Coll1 deposition (**E**) and a slight or no increase in Coll3 (**F**). **G**, **H** Matrix Metalloproteinases (MMPs), MMP-2 expressions were elevated significantly in 5 and 20 K/cm^2 iMSCs groups (**G**), while MMP-9 was reduced in all treatment groups. Data is representative of three independent experiments ($N = 3$). Data is presented as mean ± SEM, P * <0.05, ** <0.005, *** <0.0005,**** <0.0001.

skin injuries, even severe ones, we still can depend on the resident skin stem/progenitor cells for regeneration, deep burns are often associated with complete loss of these natural repairing agents[6]. Generally, autologous split-thickness skin grafts harvested from healthy donor sites are used to solve these problems and cover the wounds. However, in non-ideal cases such as large burns with limited donor site or in the presence of bacterial load on the wound bed, this treatment option is not always feasible, leaving no other choice but to temporarily cover the wound with alternatives such as allografts, xenografts or synthetic dermal substitutes each of which has its own biological and logistic complications[6]. All these limitations, together with the rise of stem cell therapy, advocate stem cell application either directly or within a matrix to stimulate and guide the burn healing process.

The development of induced pluripotent stem cells (iPSCs) by the Yamanaka group in 2006 marked a new era in regenerative medicine, opening the door for limitless possibilities for the treatment of diseases once thought incurable[30]. From a translational perspective, inducing differentiation of functional MSCs from iPSCs (iMSCs) stands out as their most prominent advantage. A multitude of research reports have shown that these iMSCs can effectively replace their native MSC counterparts for the treatment of several pathologies[31]. Even more, iMSCs showed a superior characteristic compared to primary MSCs, where they showed superior proliferation, angiogenic induction, and overall wound-healing properties[32–34]. A recent report has shown that cumulative passaging of iMSCs can produce up to a thousand times greater number of cells[20]. Another major translational obstacle regarding primary MSCs is that they show significant variations from one tissue to another in the same donor, causing inconsistencies and variability in their therapeutic outcomes, while on the other hand, iMSC generated from the same iPSC clone are homogenous, having a consistent molecular profile, and widely stable biological performance[31,35]. Such qualities strongly suggest iMSCs as an ideal stem cell candidate for treating burn wounds.

Porcine models are the closest animal wound models that resemble human wound healing and, therefore, are used to mimic the burn healing process[9,36]. The chosen cell application technique is to seed our stem cells with different doses on Integra™ sheets, a method that has proven its effectiveness in previous studies[9]. Importantly, a previous report showed that lower doses of MSCs efficiently improved burn wound healing compared to higher doses when applied on Integra™ sheets in the pig thermal injury model[25]. This data presented a shift from the traditionally held concept of proportional correlation between stem cell dose and their therapeutic effectiveness. Therefore, here, a similar dosage range of 5,10, and 20000 (5,10, and 20 K) calls per cm^2 was utilized. Indeed, the results indicated that a medium dose of 10 K cells/cm^2 showed nearly consistently better healing outcomes compared to other iMSCs doses and controls as well.

As expected, applying iMSCs to the porcine burn model proved valuable for treating burn wounds. From the perspective of wound healing kinetics, wounds treated with iMSCs demonstrated an accelerated wound closure rate that corresponded properly to the rate of re-epithelization, suggesting that the healing process is driven mainly by the formation of new epithelized tissue rather than contraction of wound edges. Indeed, iMSCs-treated wounds showed a lower contracture rate than the control groups. Naturally, during the wound re-epithelization process, epithelial cells migrate and meet at the center of the wound site, covering the laid-down granulation tissue[37]. This process is carried out primarily by stem/progenitor cells in sweat glands and pilosebaceous units in the epidermis. However, as mentioned above, the full-thickness burn injury involves the destruction of these structures and a complete loss of their cells. Alternatively, in such cases, re-epithelialization occurs through the migration of epidermal cells at wound margins, causing significant wound contraction and ultimately resulting in post-injury scarring[38]. Apparently, iMSCs could replace the lost epidermal cells and lead the reepithelization process, filling the wound site with less cellular migration needed from the keratinocyte cells as the wound margins manifested in less wound contraction, which might explain that iMSCs-treated wounds showed an overall less scar scoring than the control groups, despite being nonsignificant.

Another hallmark of assessing the wound healing quality is the ability to restore the skin's morphological features. One such feature is the presence of rete ridges, the epithelial protrusions that form at the junction of the epidermis into the dermis as a characteristic ingredient of human and pig skin[39]. These ridges are known to play an important role in maintaining skin integrity, and their formation is an indication of the basement membrane reconstruction and therefore prevents skin from shearing[40,41]. Interestingly, iMSCs-treated wounds exhibited a significant ability to re-form those ridges, indicating a sound integration between the regenerated epidermis and dermis. Additionally, iMSCs treatment induced a significant amount of collagen deposition in the underlying dermis. iMSCs-treated wounds, especially 10 K/cm^2, displayed dense and wavy collagen fibers that closely resembled the characteristic appearance in normal skin dermis.

To further investigate the mechanism of action of iMSCs in the wound healing process, their effect on the expression of key markers involved in the healing process was analyzed[42]. Importantly, iMSCs demonstrated a general suppressive effect on major proinflammatory cytokines IL-1β, while exerting a mild, non-significant influence on IL-4 and TNF-α. This suggests that iMSCs contribute to modulating a balanced inflammatory response, potentially preventing persistent hyperinflammation—a hallmark of chronic, non-healing wounds characterized by sustained elevation of these cytokines[43]. This inflammation-modulating trait is of paramount importance in burn injuries, where elevated levels of IL-1β and TNF-α are particularly associated with poor prognosis[44]. Collagen deposition is another prominent feature of a sound wound healing process[45]. In this context, iMSCs appeared to induce a preferential deposition of Collagen 1 fibers over Collagen 3. Of note, the replacement of Collagen 3 with Collagen 1, a stiffer fibrillar protein, is a benchmark of optimal wound healing[42]. Therefore, the Collagen1/3 ratio provides an estimation of the effectiveness of the wound healing process[46]. All iMSC-treated groups showed higher ratios than the control, indicating a tendency toward the normal healing pathway. To ensure this, the collagen and other fibers are remodeled to avoid excessive deposition that may lead to hypertrophic scarring, a common post-burn complication. This is regulated through the coordination between matrix metalloproteinases (MMPs) and (TIMPS)[42]. In particular, Gelatinases, MMP-2, and MMP-9 are known as major regulators of wound remodeling and angiogenesis[47]. Interestingly, iMSCs significantly reduced the expression levels of MMP-9. Increased levels of MMP-9 have been reported at the site of injury early after burn injury; however, MMP-9 remained elevated in non-healing wounds[48]. On the other hand, MMP-2 is more delicate in action as it is involved in regulating angiogenesis, inflammation, and fibrosis[47]. Interestingly, iMSCs induced a moderate increase in MMP-2 expression that might be favorable for angiogenic induction while not being highly over-expressed enough to induce fibrosis or persistent inflammation. Furthermore, plasminogen activator inhibitor-1 (PAI-1; SERPINE1), one of the serine protease inhibitor family (SERPIN) is known to orchestrate the proteolytic action of tissue proteases to fine-tune the wound remodeling[49,50] showed an increased level of iMSCs treatment, indicating that iMSCs show an overall paracrine effect that augments the healing process by modulating an adequate inflammatory response, collagen deposition and remodeling, and a pro-angiogenic capacity.

A certain limitation of the study is the relatively small sample size of $N = 3$ with 4 replicates per biological sample (i.e., iMSCs dose). However, due to limited cell availability, time constraints, and high costs, such a sample size is generally considered acceptable in stem cell research, especially for reports that include in vivo models[8,25,51,52]. Therefore, while the sample size might not allow for conclusive evidence about iMSCs' mechanism of action and role during the wound healing process, it highlights their general potential as a source for skin regeneration. Additionally, this study only used cord tissue-derived iPSCs for the generation of iMSCs to avoid confounding. It remains unclear whether iMSCs derived from other somatic cell sources, especially those derived from adult individuals, possess the same differentiation capacities and functional properties as the CT-iMSC used in this study. A variety of factors, such as the donor's age and health status, are likely to affect the yield of extracted cells as well as their functionality. However, this study can pave the way to much-needed new approaches for stem cell therapy in burn treatments.

In conclusion, we demonstrated the effectiveness of using induced mesenchymal stem cells in burn treatment and wound management. Future studies are required to explore the full spectrum of induced stem cell therapy in burn injuries. Other favorable, more accessible cell sources for iPSCs reprogramming like urine, and hair follicle cells, could serve as a renewable source of patient-specific pluripotent cells opening the gate for an individualized treatment approach[53,54].

Methods

Ethics approval and consent to participate

All protocols were approved by the Research Ethics Board and the Ethical Committee of the Sunnybrook Research Institute in the Sunnybrook Health Science Centre affiliated with the University of Toronto (Study approval number, REB #017-2011) Title of approved project: In vitro generation and characterization of mesenchymal and epithelial stem cells from the amniotic membrane and sub-amniotic umbilical cord lining membrane)(Approval date: March 1st, 2011). Ethics approval for umbilical cord collection and CT-iPSCs research was obtained from the Research Ethics Board at Mt. Sinai Hospital. (Study approval number, REB #13-0346-E). Title of approved project: The Regenerative Potential of Umbilical Cord Tissue. (Approval date: January 10th, 2014). Animal (Pig) procedures were reviewed and approved by Sunnybrook Research Institute and Sunnybrook Health Sciences Centre animal care and use committee (AUP #: 16–600). Title of approved protocol: Investigation of the effects of polysaccharide-based materials and mesenchymal stem cells on wound healing in pigs. All controlled drug exemptions were obtained from Health Canada (44219.11.17, 44220.11.17) under the Controlled Drugs and Substances Act.

Differentiation of mesenchymal stem cells from iPSCs

Human cord-tissue iPSCs used in this study were previously generated and characterized by Mohammed et al.[21]. CT-iPSCs were maintained in mTeSR7 media (StemCell Technologies) in culture dishes coated with cell attachment matrix Matrigel (BD Biosciences). The medium was changed every other day. Mesenchymal stem cell differentiation was induced according to a previously published protocol[22]. First, for mesodermal induction, cells were incubated with a mesodermal induction medium consisting of DMEM/F12 (Gibco) supplemented with 20% knockout serum replacement (KOSR) (Thermo Fisher), 1% Non-essential amino acids (NEAA) (Gibco), 5 μM/mL CHIR99021 (Sigma), 5 ng/mL activin A (Peprotech), and 20 ng/mL BMP4 (sigma) for two days. Next, cells were switched to a mesenchymal induction medium consisting of α-MEM (Gibco) supplemented with 10% knockout serum replacement (KOSR) (Thermo Fisher), 10 ng/mL bFGF (Sigma), and 10 ng/mL EGF (R&D Systems) for another ten days. On day 13, differentiated stem cells were maintained in an MSC medium of DMEM-high glucose (Gibco) supplemented with 10% FBS (Thermo Fisher), 2 mM L-glutamine (Sigma), and 1% Antibiotic-antimycotic (AbAm) (Gibco), being used in further experiments.

iMSC characterization

The immunophenotype of iMSCs was confirmed according to the *ISCT* panel. The expression of positive markers CD 105 (APC), CD 90 (PC7), CD

73 (PE), and the negative marker CD45 (FITC) was assessed using BD® LSR II Flow Cytometer and analyzed on FlowJo™ Software v10 (Becton, Dickinson & Company).

In vitro differentiation

Adipogenic differentiation: iMSCs were seeded in 6-well plates at 6000/cm^2 in adipogenic induction medium (StemPro® Adipogenesis Differentiation Kit/Gibco) and placed in an incubator at 37 °C in 5% CO_2 for 14 days with media changes twice weekly. To assess adipogenesis, cells were rinsed with PBS, fixed in 10% formalin for 30 min, rinsed with distilled water, and stained with Oil Red O (Sigma) for 5 min at room temperature. Cells were counterstained with hematoxylin (Sigma). Cells were imaged under a microscope (Lionheart).

Osteogenic differentiation: iMSCs were seeded in 6-well plates at 6000 cells/cm^2 in an osteogenic induction medium (StemPro® Osteogenesis Differentiation Kit/Gibco) and placed in an incubator at 37 °C in 5% CO_2 for 21 days, with media changes twice weekly. To confirm osteogenic differentiation, cells were rinsed with PBS, fixed in 10% formalin for 30 min, rinsed with distilled water, and stained with Alizarin red (Sigma-Aldrich) in the dark for 45 min. Cells were washed with distilled water before imaging.

Chondrogenic differentiation: 500,000 cells/mL iMSCs were aliquoted in chondrogenic media (StemPro® Chondrogenesis Differentiation Kit/Gibco) and pelleted by centrifugation at 300 g in a 15 mL Falcon tube for 5 min at room temperature. The caps of the falcon tubes were loosened and placed in an incubator at 37 °C in 5% CO_2 for 21 days. The medium was changed three times weekly without disrupting the cell pellet. To confirm chondrogenesis, cell pellets were fixed in 10% formalin for 24 h and then placed in 70% ethanol for an additional 24 h. Aggregates were embedded in paraffin, then cut into 5 µm slices, and placed on microscope slides. Sections were stained with 1% alcian blue 3GX (Santa Cruz Biotechnology) in 3% acetic acid in water for 30 min at RT. The stain was washed with tap water, then distilled water, then counterstained with 0.1% nuclear fast red (Santa Cruz Biotechnology) before imaging.

Immunocytochemistry

For iPSCs and iMSCs staining, cells were seeded onto either Geltrex-coated or non-coated 12-well plates for iPSCs and iMSCs, respectively. Cells were cultured till confluency, washed twice with PBS, and then fixed with 10% formalin for 20 min at room temperature. Next, cells were washed with PBS and blocked for non-specific antibody binding with blocking buffer (10% FBS, 0.1% in PBS) for 30 min at room temperature, followed by incubation with the primary antibodies diluted with antibody buffer (0.2% FBS, 0.1% Triton X-100 in PBS). The following primary antibodies were used: intracellular pluripotency markers; Sox2 (1:100, R&D Systems), Nanog (1:10, ReproCell)[55], and mesodermal markers; EOMES (1:100, Invitrogen), and MIXL1(1:50, Invitrogen)[23,24]. All Primary antibodies were incubated overnight at 4 °C. After the incubation period, the cells were washed 4X for 15 min, and each respective secondary antibody was added to the cells and then incubated for 30 min at room temperature in the dark. Next, the cells were washed for 5X for 15 min and stained with DAPI. All fluorescence images were taken on the spinning disk confocal (Quorum WaveFX Spinning Disc Confocal System).

iMSC seeding on Integra® dermal regeneration template

Cell suspensions in varying concentrations (5, 10, and 20 K per cm^2) were pipetted onto the bovine collagen layer and later placed directly onto the wound bed according to an established wound care protocol[56] (Fig. 1). Cells were seeded on Integra® using an 8-channel pipette with a cell concentration ranging from 1.56×105 to 6.25×105 cells/mL (for 5000, 10,000, and 20,000 cells/cm^2 seeding densities) on the dermal side with the silicone side facing down (Fig. 1). Cells were allowed to attach in a humidified incubator at 37 °C at 5% CO_2 for 2 h, before completely submerging in a complete medium for 48 h. Cell-seeded Integra® was washed in Ringer's lactate solution before transplantation on porcine burn wounds.

Porcine thermal injury model

All animal procedures were performed on female Yorkshire pigs (25–30 kg, Colwell Farms, Ontario, Canada) under protocols approved by the Animal Policy and Welfare Committee of the University of Toronto, Sunnybrook Research Institute, and Sunnybrook Health Sciences Centre Animal Care and Use Committee. All pigs were acclimatized for at least 2 weeks before thermal injury. Under anesthesia, (initially 0.2 mg/kg subcutaneous ketamine combined with 0.5–1.0 mg atropine 0.5–1.0 mg to control the heart rate and continuous 5%/l/O_2 isoflurane through endotracheal intubation) and analgesia (0.05 mg/kg subcutaneous buprenorphine), 5 × 5 cm dorsal full-thickness burns were created using a heated aluminum device (200 °C) for 20 seconds under a constant force of 4 N measured using a digital force gauge (Mark-10 Corporation). These parameters (heating temperature and application time)were chosen based on a previously established and published protocol[56]. A 5 cm interspace was maintained between adjacent wounds. The wounds were covered with paraffin gauze and wet-to-dry gauze dressings and kept in place by skin staples, an adhesive bandage, and an elastic stocking porcine suit. After 48 h (day 0), the burned skin was excised up to the fascia. The resulting 5 × 5 cm full-thickness excisional wounds were then covered with scaffolds. Wounds were randomized and assigned to a total of five groups; burn alone and acellular Integra® served as control groups, and the three test groups consisted of Integra® seeded with varying concentrations of iMSCs (5×10^3, 10×10^3, and 20×10^3 cells/cm^2, labelled 5K-iMSC, 10K-iMSCs, and 20K-iMSCs, respectively) ($N = 5$) on the back of each of three Yorkshire pigs (Fig. 1). All wounds (control and test groups) were covered by layers of fatty gauze, wet gauze, dry gauze, and an abdominal pad, which were secured by sterile skin staples and adhesive bandages. Further, a swine jacket and fitted spandex were applied to protect the bandages. During regular dressing changes every 3–7 days, wounds were monitored for adverse events and wound healing and photo-documented for evaluation. On day 40, skin biopsies were obtained for histochemical and molecular analysis, and animals were euthanized by injection of 480 mg/kg pentobarbital while under general anesthesia. Wound images at each time point were used for gross appearance and wound area analysis using ImageJ software (NIH). Wound closure was calculated as the remaining percentage area of the original wound. The wound closure rate was calculated using the following equation: % Wound closure = [(Day 0 wound area − Day X wound area)/Day 0 wound area] × 100.

Wound scar assessment

The scar quality was assessed by external blinded surgeons on day 40 using the Vancouver Scar Scale, a validated 5-item scoring tool encompassing vascularity, pigmentation, pliability, and height.

Histochemical and Immunohistochemical analysis

Histological skin biopsies were fixed in 10% formalin for 48 h at room temperature and stored in 70% ethanol at 4 °C until serial sectioning (5 µm thickness) at SRI Histology Core. Histological sections were stained with hematoxylin and eosin (H&E) for morphological analysis and Masson's Trichrome for analyzing collagen density. Each section's average epidermis thickness, rete ridges, and cell number were calculated from the mean value from five random areas. Stained slides were imaged under a Leica light microscope (LEICADM 2000 LED) and analyzed with the evaluator blinded to treatment/control conditions. Histological images were analyzed using ImageJ software by thresholding RGB images and converting

Table 1 | Primer sequence for qPCR (Pig)

Gene (pig)	Forward sequence	Reverse sequence
IL4	CTCCCAACTGATCCCAACCC	TGCACGAGTTCTTTCTCGCT
Coll1α1	CTCCTGGTATTGCTGGTGCT	CACAGTGTCTCCTTGCTGCG
Coll 3	CTAGCCGAGCTTCCCAGAAC	CCCCATTCCCCAGTGTGTTT
MMP2	AGGATGGCAAGTACGGCTTC	AGCTGTTGTAGGATGTGCCC
MMp9	CATTCAAGGAGACGCCCACT	GCCTTTTGCGTTTCCGAAGT
IL6	CCGCGGCCTGAGAGAAATA	GGGCTGATATGACCACATGGA
IL1β	TGCCACCTTTTGACAGTGATG	TGATGTGCTGCTGCGAGATT
TNF-α	AACTGTAGGTTGCTCCCACC	GACCAGTAGGGCGGTTACAG
TGFβ3	GGCTGTCCTTTGATGTCACC	GGCCAGAATTGAACCCGT
TNC	CACCATCCTCCTCACAGCAG	GTAAAGGTCTCGAAGGCCCC
VEGF	ATCACGAAGTGGTGAAGTTC	TGCTGTAGGAAGCTCATCTC
PAI1	GCAACGTGGTTTTCTCACCC	TTGTACAGTTGACGGAGGGC
GAPDH	GTCGGAGTGAACGGATTTGGC	CTTGCCGTGGGTGGAATCAT

them to grayscale to determine collagen density and the number of infiltrating cells.

Quantitative PCR (qPCR)

Total RNA was isolated from skin samples from day 40 using TRI Reagent (Sigma), according to the manufacturer's instructions. cDNA was synthesized using the high-capacity cDNA reverse transcription kit (Applied Biosystems). Real-time quantitative PCR was performed using the RT-Real-Time iTaq™ Universal SYBR® Green Supermix (Bio-Rad) with specific primers (Table 1). Gene expression was calculated through the formula ΔΔCt = ΔCt of test sample - ΔCt of the control sample, where ΔCt = Ct gene studied – Ct 18 s (housekeeping gene, used as an internal control of the reaction).

Data analysis

Data was analyzed with one-way ANOVA, followed by Turkey test or Bonferroni multiple comparison test, to determine the significance of differences. Values were considered significant at $P < 0.05$. All data were analyzed with Prism9 (GraphPad) and is shown as mean ± standard error of the mean (SEM).

Data availability

Original flow cytometry data, microscopy data, or any additional information required to reanalyze the data reported in this paper will be shared by the lead contact upon request. All additional files are included in the manuscript. Further information and resource requests should be directed to the Lead Contact, Dr. Marc G. Jeschke (marc.jeschke@hhsc.ca).

Received: 21 April 2025; Accepted: 13 August 2025;
Published online: 30 August 2025

References

1. Smolle, C. et al. Recent trends in burn epidemiology worldwide: A systematic review. *Burns* **43**, 249–257 (2017).
2. Jeschke, M. G. et al. Burn injury. *Nat. Rev. Dis. Prim.* **6**, 11 (2020).
3. El Khatib, A. & Jeschke, M. G. Contemporary Aspects of Burn Care. *Medicina (Kaunas)* **57**, https://doi.org/10.3390/medicina57040386 (2021).
4. Chang, D. K., Louis, M. R., Gimenez, A. & Reece, E. M. The Basics of Integra Dermal Regeneration Template and its Expanding Clinical Applications. *Semin. Plast. Surg.* **33**, 185–189 (2019).
5. Petrus-Reurer, S. et al. Immunological considerations and challenges for regenerative cellular therapies. *Commun. Biol.* **4**, https://doi.org/10.1038/s42003-021-02237-4 (2021).
6. Abdul Kareem, N., Aijaz, A. & Jeschke, M. G. Stem Cell Therapy for Burns: Story so Far. *Biologics: Targets Ther.* **15**, 379–397 (2021).
7. Jeschke, M. G., Rehou, S., McCann, M. R. & Shahrokhi, S. Allogeneic mesenchymal stem cells for treatment of severe burn injury. *Stem Cell Res. Ther.* **10**, https://doi.org/10.1186/s13287-019-1465-9 (2019).
8. Dolp, R. et al. Biological characteristics of stem cells derived from burned skin—a comparative study with umbilical cord stem cells. *Stem Cell Res. Ther.* **12**, https://doi.org/10.1186/s13287-021-02140-z (2021).
9. Amini-Nik, S. et al. Stem cells derived from burned skin - The future of burn care. *EBioMedicine* **37**, 509–520 (2018).
10. Roobrouck, V. D., Ulloa-Montoya, F. & Verfaillie, C. M. Self-renewal and differentiation capacity of young and aged stem cells. *Exp. Cell Res.* **314**, 1937–1944 (2008).
11. Jo, H. et al. Applications of Mesenchymal Stem Cells in Skin Regeneration and Rejuvenation. *Int. J. Mol. Sci.* **22**, 2410 (2021).
12. Cerneckis, J., Cai, H. & Shi, Y. Induced pluripotent stem cells (iPSCs): molecular mechanisms of induction and applications. *Sig. Trans. Target. Ther.* **9**, https://doi.org/10.1038/s41392-024-01809-0 (2024).
13. Robinton, D. A. & Daley, G. Q. The promise of induced pluripotent stem cells in research and therapy. *Nature* **481**, 295–305 (2012).
14. Xu, M., Shaw, G., Murphy, M. & Barry, F. Induced Pluripotent Stem Cell-Derived Mesenchymal Stromal Cells Are Functionally and Genetically Different From Bone Marrow-Derived Mesenchymal Stromal Cells. *Stem Cells* **37**, 754–765 (2019).
15. Dominici, M. et al. Minimal criteria for defining multipotent mesenchymal stromal cells. The International Society for Cellular Therapy position statement. *Cytotherapy* **8**, 315–317 (2006).
16. Deuse, T. et al. Hypoimmunogenic derivatives of induced pluripotent stem cells evade immune rejection in fully immunocompetent allogeneic recipients. *Nat. Biotechnol.* **37**, 252–258 (2019).
17. Araki, R. et al. Negligible immunogenicity of terminally differentiated cells derived from induced pluripotent or embryonic stem cells. *Nature* **494**, 100–104 (2013).
18. Lian, Q. et al. Functional Mesenchymal Stem Cells Derived From Human Induced Pluripotent Stem Cells Attenuate Limb Ischemia in Mice. *Circulation* **121**, 1113–1123 (2010).
19. Soontararak, S. et al. Mesenchymal Stem Cells (MSC) Derived from Induced Pluripotent Stem Cells (iPSC) Equivalent to Adipose-Derived MSC in Promoting Intestinal Healing and Microbiome Normalization in Mouse Inflammatory Bowel Disease Model. *Stem Cells Transl. Med.* **7**, 456–467 (2018).

20. Lee, H.-R. et al. iPSC-Derived MSCs Are a Distinct Entity of MSCs with Higher Therapeutic Potential than Their Donor-Matched Parental MSCs. *Int. J. Mol. Sci.* **24**, 881 (2023).
21. Mohamed, A. et al. Umbilical Cord Tissue as a Source of Young Cells for the Derivation of Induced Pluripotent Stem Cells Using Non-Integrating Episomal Vectors and Feeder-Free Conditions. *Cells* **10**, https://doi.org/10.3390/cells10010049 (2020).
22. Tran, N. T., Trinh, Q. M., Lee, G. M. & Han, Y. M. Efficient differentiation of human pluripotent stem cells into mesenchymal stem cells by modulating intracellular signaling pathways in a feeder/serum-free system. *Stem Cells Dev.* **21**, 1165–1175 (2012).
23. Stavish, D. et al. Generation and trapping of a mesoderm biased state of human pluripotency. *Nat. Commun.* **11**, https://doi.org/10.1038/s41467-020-18727-8 (2020).
24. Arnold, S. J., Hofmann, U. K., Bikoff, E. K. & Robertson, E. J. Pivotal roles for eomesodermin during axis formation,epithelium-to-mesenchyme transition and endoderm specification in the mouse. *Development* **135**, 501–511 (2008).
25. Eylert, G. et al. Skin regeneration is accelerated by a lower dose of multipotent mesenchymal stromal/stem cells—a paradigm change. *Stem Cell Res. Ther.* **12**, https://doi.org/10.1186/s13287-020-02131-6 (2021).
26. Bates-Jensen, B. M., McCreath, H. E., Harputlu, D. & Patlan, A. Reliability of the Bates-Jensen wound assessment tool for pressure injury assessment: The pressure ulcer detection study. *Wound Repair Regeneration* **27**, 386–395 (2019).
27. Xiao, T., Yan, Z., Xiao, S. & Xia, Y. Proinflammatory cytokines regulate epidermal stem cells in wound epithelialization. *Stem Cell Res. Ther.* **11**, https://doi.org/10.1186/s13287-020-01755-y (2020).
28. Dolp, R. et al. Biological characteristics of stem cells derived from burned skin-a comparative study with umbilical cord stem cells. *Stem Cell Res Ther.* **12**, 137 (2021).
29. Jeschke, M. G. et al. Pathophysiologic Response to Severe Burn Injury. *Ann. Surg.* **248**, 387–401 (2008).
30. Takahashi, K. & Yamanaka, S. Induction of Pluripotent Stem Cells from Mouse Embryonic and Adult Fibroblast Cultures by Defined Factors. *Cell* **126**, 663–676 (2006).
31. Dias, I. X., Cordeiro, A., Guimarães, J. A. M. & Silva, K. R. Potential and Limitations of Induced Pluripotent Stem Cells-Derived Mesenchymal Stem Cells in Musculoskeletal Disorders Treatment. *Biomolecules* **13**, 1342 (2023).
32. Eto, S. et al. Mesenchymal stem cells derived from human iPS cells via mesoderm and neuroepithelium have different features and therapeutic potentials. *PLOS ONE* **13**, e0200790 (2018).
33. Wei, H. et al. One-step derivation of cardiomyocytes and mesenchymal stem cells from human pluripotent stem cells. *Stem Cell Res* **9**, 87–100 (2012).
34. Wang, Q. et al. Comparative analysis of mesenchymal stem/stromal cells derived from human induced pluripotent stem cells and the cognate umbilical cord mesenchymal stem/stromal cells. *Heliyon* **9**, e12683 (2023).
35. Zhang, C. et al. Eradication of specific donor-dependent variations of mesenchymal stem cells in immunomodulation to enhance therapeutic values. *Cell Death Dis.* **12**, https://doi.org/10.1038/s41419-021-03644-5 (2021).
36. Singer, A. J. et al. Effects of burn location and investigator on burn depth in a porcine model. *Burns* **42**, 184–189 (2016).
37. Chen, D., Hao, H., Fu, X. & Han, W. Insight into Reepithelialization: How Do Mesenchymal Stem Cells Perform?. *Stem Cells Int.* **2016**, 1–9 (2016).
38. Rousselle, P., Braye, F. & Dayan, G. Re-epithelialization of adult skin wounds: Cellular mechanisms and therapeutic strategies. *Adv. Drug Deliv. Rev.* **146**, 344–365 (2019).
39. Shen, Z. et al. Rete ridges: Morphogenesis, function, regulation, and reconstruction. *Acta Biomater.* **155**, 19–34 (2023).
40. Lin, C. H. et al. Regeneration of rete ridges in Lanyu pig (Sus scrofa): Insights for human skin wound healing. *Exp. Dermatol* **28**, 472–479 (2019).
41. Carney, B. C. et al. Rete ridges are decreased in dyschromic burn hypertrophic scar: A histological study. *Burns* **50**, 66–74 (2024).
42. Faour, S., Farahat, M., Aijaz, A. & Jeschke, M. G. Fibrosis in burns: an overview of mechanisms and therapies. *Am. J. Physiol. Cell Physiol.* **325**, C1545–C1557 (2023).
43. Wang, Z., Qi, F., Luo, H., Xu, G. & Wang, D. Inflammatory Microenvironment of Skin Wounds. *Front. Immunol.* **13**, https://doi.org/10.3389/fimmu.2022.789274 (2022).
44. Dejesus, J. E., Wen, J. J. & Radhakrishnan, R. Cytokine Pathways in Cardiac Dysfunction following Burn Injury and Changes in Genome Expression. *J. Personalized Med.* **12**, 1876 (2022).
45. Landén, N. X., Li, D. & Ståhle, M. Transition from inflammation to proliferation: a critical step during wound healing. *Cell. Mol. Life Sci.* **73**, 3861–3885 (2016).
46. Singh, D., Rai, V. & Agrawal, D. K. Regulation of Collagen I and Collagen III in Tissue Injury and Regeneration. *Cardiol. Cardiovasc Med* **7**, 5–16 (2023).
47. Caley, M. P., Martins, V. L. C. & O'Toole, E. A. Metalloproteinases and Wound Healing. *Adv. Wound Care* **4**, 225–234 (2015).
48. Sharma, C., Dobson, G. P., Davenport, L. M., Morris, J. L. & Letson, H. L. The role of matrix metalloproteinase-9 and its inhibitor TIMP-1 in burn injury: a systematic review. *Int J. Burns Trauma* **11**, 275–288 (2021).
49. Simone, T. & Higgins, P. Inhibition of SERPINE1 Function Attenuates Wound Closure in Response to Tissue Injury: A Role for PAI-1 in Re-Epithelialization and Granulation Tissue Formation. *J. Developmental Biol.* **3**, 11–24 (2015).
50. Simone, T. M. et al. SERPINE1: A Molecular Switch in the Proliferation-Migration Dichotomy in Wound-"Activated" Keratinocytes. *Adv. Wound Care* **3**, 281–290 (2014).
51. Reinisch, A. et al. Epigenetic and in vivo comparison of diverse MSC sources reveals an endochondral signature for human hematopoietic niche formation. *Blood* **125**, 249–260 (2015).
52. Fujiwara, T. et al. Age-associated intracellular superoxide dismutase deficiency potentiates dermal fibroblast dysfunction during wound healing. *Exp. Dermatol.* **28**, 485–492 (2019).
53. Yin, X. et al. Exploiting urine-derived induced pluripotent stem cells for advancing precision medicine in cell therapy, disease modeling, and drug testing. *J. Biomed. Sci.* **31**, https://doi.org/10.1186/s12929-024-01035-4 (2024).
54. Klingenstein, S., Klingenstein, M., Kleger, A. & Liebau, S. From Hair to iPSCs—A Guide on How to Reprogram Keratinocytes and Why. *Curr. Protocols Stem Cell Biol.* **55**, https://doi.org/10.1002/cpsc.121 (2020).
55. Wang, Z., Oron, E., Nelson, B., Razis, S. & Ivanova, N. Distinct Lineage Specification Roles for NANOG, OCT4, and SOX2 in Human Embryonic Stem Cells. *Cell Stem Cell* **10**, 440–454 (2012).
56. Branski, L. K. et al. A porcine model of full-thickness burn, excision and skin autografting. *Burns* **34**, 1119–1127 (2008).

Acknowledgements

The authors would like to express their appreciation to Toronto Hydro for their generous donation and to thank members of the Rogers Lab at Lunenfeld Tanenbaum Research Institute for their invaluable support. This work was funded by the Canadian Institutes of Health Research # 123336. CFI Leader's Opportunity Fund: Project # 25407, National Institutes of Health 2R01GM087285-05A1. Ontario Institute of Regenerative Medicine.

Author contributions

M.F., S.B., and M.G.J. conceptualized the article. M.F. and S.B. designed, performed, and analyzed experiments. M.F. wrote and edited the manuscript. A.A., B.C., Y.C., G.R., M.E., and M.F.H. performed specific

experiments. I.M.R. edited the manuscript and provided critical advice. M.G.J. designed experimental outlines, edited, and approved the manuscript.

Competing interests
The authors declare no competing interests.

Additional information
Supplementary information The online version contains supplementary material available at https://doi.org/10.1038/s41536-025-00427-w.

Correspondence and requests for materials should be addressed to Marc G. Jeschke.